Title	Decadal to monthly timescales of magma transfer and reservoir growth at a caldera volcano(Main article)
Author(s)	Druitt, T. H.; Costa, Fidel; Deloule, E.; Dungan, Michael; Scaillet, Bruno
Citation	Druitt, T. H., Costa, F., Deloule, E., Dungan, M., & Scaillet, B. (2012). Decadal to monthly timescales of magma transfer and reservoir growth at a caldera volcano. Nature, 482, 77–80.
Date	2012
URL	http://hdl.handle.net/10220/7536
Rights	© 2012 Macmillan Publishers Limited. This is the author created version of a work that has been peer reviewed and accepted for publication by Nature, Nature Publishing Group, a division of Macmillan Publishers Limited. It incorporates referee's comments but changes resulting from the publishing process, such as copyediting, structural formatting, may not be reflected in this document. The published version is available at: [DOI: http://dx.doi.org/10.1038/nature10706].

Decadal to monthly timescales of magma transfer and reservoir growth at a caldera volcano

T. H. Druitt[1,2,3], F. Costa[4], E. Deloule[5], M. Dungan[6] & B. Scaillet[7]

Caldera-forming volcanic eruptions are low-frequency, high-impact events capable of discharging tens to thousands of cubic kilometres of magma explosively on timescales of hours to days, with devastating effects on local and global scales[1]. Because no such eruption has been monitored during its long build-up phase, the precursor phenomena are not well understood. Geophysical signals obtained during recent episodes of unrest at calderas such as Yellowstone, USA, and Campi Flegrei, Italy, are difficult to interpret, and the conditions necessary for large eruptions are poorly constrained[2,3]. Here we present a study of pre-eruptive magmatic processes and their timescales using chemically zoned crystals from the 'Minoan' caldera-forming eruption of Santorini volcano, Greece[4], which occurred in the late 1600s BC. The results provide insights into how rapidly large silicic systems may pass from a quiescent state to one on the edge of eruption[5,6]. Despite the large volume of erupted magma[4] (40–60 cubic kilometres), and the 18,000-year gestation period between the Minoan eruption and the previous major eruption, most crystals in the Minoan magma record processes that occurred less than about 100 years before the eruption. Recharge of the magma reservoir by large volumes of silicic magma (and some mafic magma) occurred during the century before eruption, and mixing between different silicic magma batches was still taking place during the final months. Final assembly of large silicic magma reservoirs may occur on timescales that are geologically very short by comparison with the preceding repose period, with major growth phases immediately before eruption. These observations have implications for the monitoring of long-dormant, but potentially active, caldera systems.

Crystals in volcanic rocks provide records of magma reservoir processes and timescales before eruptions[7]. A crystal growing from a magmatic melt incorporates trace elements in quantities governed by thermodynamic and kinetic laws[8,9]. If the crystal is subsequently mixed into another melt, trace elements that diffuse sufficiently fast will begin to re-equilibrate with the new host melt, generating intracrystalline diffusion gradients than can be used to obtain time information[10–12] (Supplementary Fig. 1).

A novel technique for extracting multiple timescales from single crystals has been applied to plagioclase crystals in rhyodacitic (71–72 wt% SiO_2) pumices from the Minoan eruption. The pumices from all four phases of the eruption (phase 1, Plinian; phases 2 and 3, phreatomagmatic; phase 4, ignimbrite[13]) contain ~10 vol% crystals set in rhyolitic[13] (73–74 wt% SiO_2) glass. Plagioclase is the dominant crystalline phase, the others being orthopyroxene, clinopyroxene, magnetite, ilmenite and apatite. It occurs as zoned crystals, whose compositional variations are dominated by charge-coupled solid solution between the endmembers, anorthite (An, $CaAl_2Si_2O_8$) and albite ($NaAlSi_3O_8$).

Two types of plagioclase have been recognized from examination of about 300 crystals (Fig. 1 and Supplementary Figs 2 and 3). A dominant type (type 1) has euhedral to partly resorbed cores of $An_{58–43}$ (58–43 mol% An) overgrown by variably developed, euhedral rims of $An_{43–36}$ containing multiple dissolution surfaces (Fig. 1a–d). The cores and rims form compositionally distinct populations (Fig. 1g). In some crystals, the cores also contain euhedral to anhedral inner cores of $An_{88–58}$ ('calcic inner cores'; Fig. 1 a, c). A spectrum of type-1 crystals is observed, from those with thick rims (up to 100 μm) to those with thin rims to those in which the rim is absent (Fig. 1f). In rimmed type-1 crystals, the plagioclase in contact with the host glass is $An_{\sim 40}$, whereas in rimless ones it is $An_{\sim 50}$ (that is, the core composition). Rimmed type-1 crystals occur in pumices from all four eruptive phases, but rimless ones have only been observed in pumices from phase 4. Type-2 crystals are very rare; they are reversely zoned, with cores of

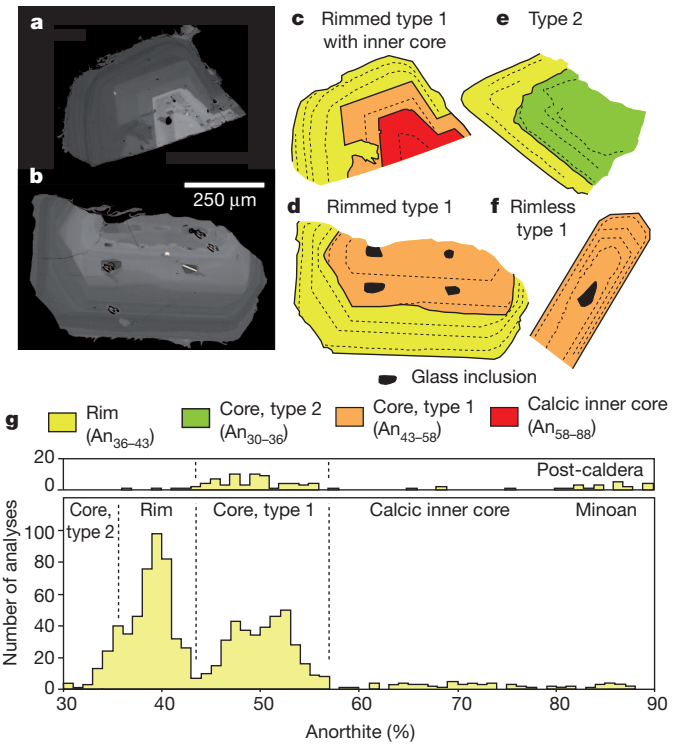

Figure 1 | Images and compositions of plagioclase crystals in Minoan pumice. a, **b**, Back-scattered electron images of two rimmed type-1 crystals (S82-30A 12 and S82-34B A2). **c**–**f**, Sketches of representative plagioclase crystals of the different types: S82-30A 12 (**c**); S82-34B A2 (**d**); S82-20D 76 (**e**); S82-20D C1 (**f**). More crystals are shown in Supplementary Fig. 2. **g**, Histogram of Minoan plagioclase compositions (bottom), based on 922 analyses, showing the different compositional groups. A histogram of plagioclase compositions from the post-caldera lavas[16,17] (top) is shown for comparison.

[1]Clermont Université, Université Blaise Pascal, Laboratoire Magmas et Volcans, BP 10448, F-63000 Clermont-Ferrand, France. [2]CNRS, UMR 6524, LMV, F-63038 Clermont-Ferrand, France. [3]IRD, R 163, LMV, F-63038 Clermont-Ferrand, France. [4]Earth Observatory of Singapore, Nanyang Technological University, Singapore 639798. [5]CRPG-CNRS, BP20, 54501 Vandoeuvre les Nancy, France. [6]Département de Minéralogie, Université de Genève, Rue des Maraîchers, 13 CH-1205 Genève, Switzerland. [7]ISTO–UMR 6113 CNRS/Université d'Orléans/Université Francois Rabelais de Tours, 1A rue de la Ferollerie, 45071 Orleans, France.

$An_{36–30}$ mantled by rims identical to those of type 1 (Fig. 1e). The broad range of plagioclase compositions in Minoan pumices shows that the rhyodacite was the product of open-system magmatic processes involving multiple, compositionally diverse magmas.

We analysed trace elements in four rimmed type-1 crystals, one rimless type-1 crystal, some interstitial glasses and some inclusions of glass contained within the crystals (Fig. 2 and Supplementary Tables 1 and 2). Magnesium (Mg), strontium (Sr) and titanium (Ti) are particularly useful elements for characterizing coexisting melt compositions and mixing timescales because they partition differently between melt and plagioclase[8] and diffuse at different rates. Mg diffuses faster than Sr (ref. 7); Ti probably diffuses slowly owing to its high charge. We used published An-dependent partition coefficients[8] to invert melt trace-element contents to those of equivalent plagioclase (Fig. 2), and vice versa (Fig. 3). Rimmed type-1 crystals have core-to-rim gradients in all three elements (Fig. 2). Rim compositions record equilibrium with interstitial glass, but concentrations of Mg, Sr and Ti in the cores and calcic inner cores are significantly higher than those calculated to be in equilibrium with the glass (Fig. 2, green lines). The rimless type-1 crystal has concentrations of Mg and Sr throughout that are too high to have been in equilibrium with the glass. None of these crystals resided in the host melt long enough for any of these elements to reach total equilibrium with the host melt.

This observation is reinforced by a comparison of calculated Mg, Ti and Sr concentrations of melts in equilibrium with the different plagioclase zones (referred to as Mg_{melt}, Ti_{melt} and Sr_{melt}, respectively), with those of Santorini lavas, pumices and glasses. The latter represent an approximate liquid line of descent of the magmatic system (Fig. 3a, b). The calculated concentrations of Sr_{melt} and Ti_{melt} span the entire range of erupted compositions, whereas those of Mg_{melt} fall below the liquid line of descent, especially in the calcic inner cores. These crystals have retained near-primary values of Sr and Ti, but Mg seems to have been partly re-equilibrated by diffusion.

We used the Sr contents of the crystals to calculate the compositions of melts from which the different zones crystallized (Fig. 3). The rims of the type-1 and type-2 crystals formed from melts with 60–90 p.p.m. Sr (71–74 wt% SiO_2), which encompasses the range of whole-rock to glass compositions of the host rhyodacite. The cores of the type-1 crystals formed from melts with 110–170 p.p.m. Sr (dacite with 63–69 wt% SiO_2), and the cores of the type-2 crystals formed from melts with 40–60 p.p.m. Sr (rhyolite with 74–76 wt% SiO_2). We interpret these observations as recording the mixing of a dacite (carrying plagioclase of the type-1 core composition) with a rhyolite (carrying plagioclase of the type-2 core composition) to generate a hybrid rhyodacite (followed by growth of the rim) that was erupted as the Minoan pumice. The rimless type-1 crystals were derived directly from the dacite, and had not resided in the hybrid rhyodacite long enough to grow rims. The calcic inner cores formed from basaltic andesite melts, with >200 p.p.m. Sr and <57 wt% SiO_2, that were mixed into the dacite at an earlier stage. The possibility that the crystal cores and inner cores are derived from older plutonic mush is not favoured on the balance of evidence (Supplementary Discussion).

The times elapsed between the different mixing events and eruption have been calculated by modelling the partial relaxation of Mg concentrations in different parts of the crystals[12] (Fig. 2 and Table 1). We first modelled the entire crystal ('one-step model'), which assumes that diffusion started only after the entire crystal had grown. Model results for the elapsed time ranged from 1 to 60 yr, but good fits could not be obtained. We therefore approximated the more realistic situation of simultaneous crystal growth and diffusion by modelling the crystals incrementally zone by zone ('two-step model'). In this manner, we obtained better overall fits to the data (Fig. 2), from which we infer that (1) a first magma mixing episode recorded by incorporation of the calcic inner cores of the type-1 crystals into the dacite occurred no more than ~100 yr before eruption; (2) a second mixing episode, or series of episodes, involving the dacite and the rhyolite occurred less than ~10 yr before eruption; and (3) the rimless type-1 crystals cannot have resided in the Minoan magma more than a few months without some diffusive loss of Mg from the rim. We have no constraints on the ages of the cores of the rare type-2 crystals. These estimates are accurate to better than one order of magnitude (Methods). The Mg-derived times were tested against the diffusive equilibration of Sr using the comprehensive diffusion data for this element (Fig. 2). Taking the measured profiles of Sr as being close to initial values, diffusion times an order of magnitude longer than those obtained from Mg would significantly blur the observed tight correlation between Sr and An contents (Fig. 3c), and are ruled out.

Our reconstruction of events, which is justified more fully in Supplementary Discussion, is as follows. During the century before eruption, dacitic magma containing crystals of calcic plagioclase began to ascend from a deep storage zone beneath Santorini, possibly pushed by injections of mafic magma (Supplementary Fig. 4). Once at shallow

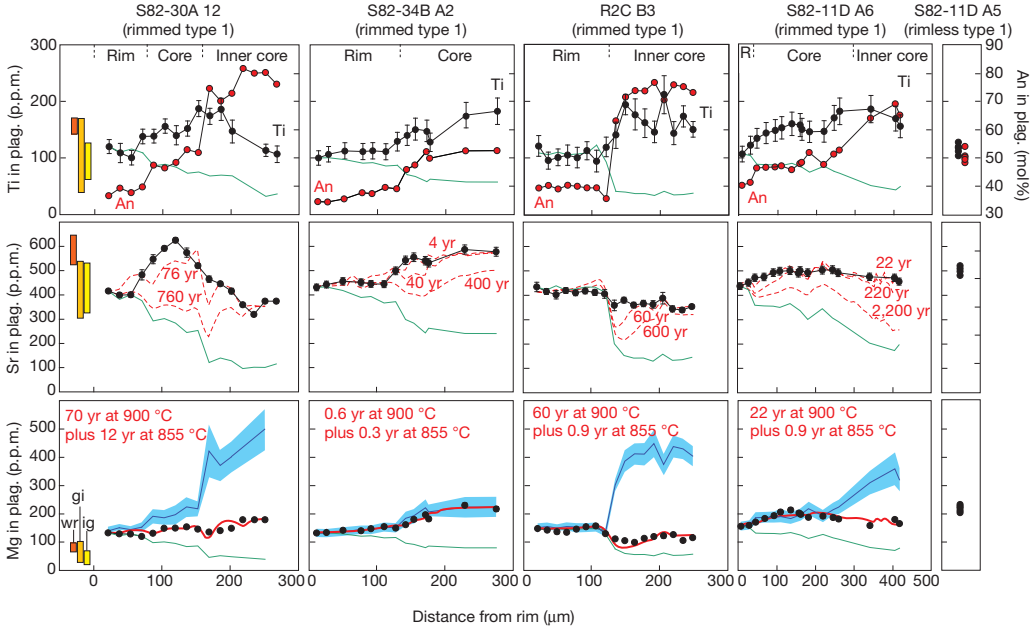

Figure 2 | Concentration–distance profiles of An (red dots) and of Sr, Ti and Mg (black dots) in Minoan plagioclase crystals. Equilibrium profiles for Sr, Ti and Mg (green lines) were calculated using published partition functions[8] at 855 °C. Calculated plagioclase compositions in equilibrium with interstitial glasses (ig), glass inclusions (gi) and whole-rock (wr) pumice compositions[13] are also shown. The blue lines in the Mg plots are the initial Mg profiles (with 1σ range). The red solid lines in the Mg plots are the best-fit two-step Mg diffusion models (time shown in years). The red dotted lines in the Sr plots are diffusion models (one-step models; 900 °C; time shown in years) in which we assume that the measured profile is close to the initial condition, as suggested by Fig. 3a. Error bars, 1σ.

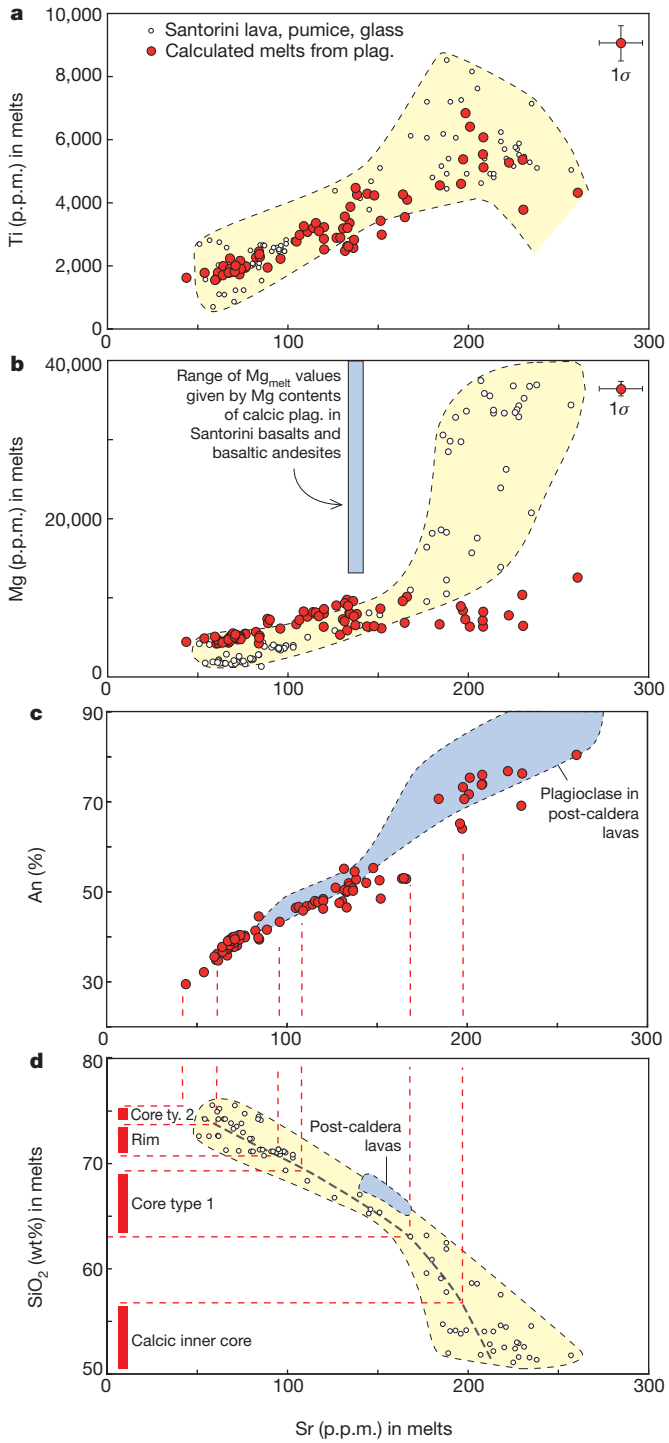

Figure 3 | Melt compositions calculated by inversion of plagioclase trace-element compositions. **a**, **b**, Ti, Mg and Sr melt contents calculated using the plagioclase–liquid partition functions of ref. 8. Temperature was obtained from $T = 855\,^{\circ}\mathrm{C} + 200\,^{\circ}\mathrm{C} \times (\%\mathrm{An} - \%\mathrm{An}_{40})/(\%\mathrm{An}_{80} - \%\mathrm{An}_{40})$, which assumes that An_{40} plagioclase crystallized at 855 °C and that An_{80} crystallized at 1,055 °C, the temperature of Santorini basaltic andesite. The values are compared with the compositional fields of Santorini cycle-2 lavas[17], Minoan pumices and Minoan glasses. The range of Mg_{melt} values calculated in the same way from the Mg contents of calcic ($An_{>80}$) plagioclase in Santorini basalts and basaltic andesites are much higher (14,000–47,000 p.p.m.) than those in the calcic inner cores of Minoan crystals, showing that the latter have lost Mg by diffusion. **c**, **d**, Use of calculated melt Sr contents from plagioclase allows estimation of the SiO_2 contents of the melts from which each plagioclase compositional group crystallized. The compositional field of plagioclases in the post-caldera lavas is taken from ref. 32.

levels, the dacite intersected one or more extant bodies of rhyolite situated at a depth of a few kilometres[14]. The cores of the type-1 crystals grew during the ascent of the dacite and/or its ponding at the base of the reservoir. Then, starting about a decade before eruption, the dacite mixed with the rhyolite to form rim overgrowths on the type-1 crystals. Mixing caused resorption of most crystals initially present in the rhyolite, and formed the hybrid rhyodacite that was subsequently erupted. Successive waves of recharge and heating of the reservoir are recorded as multiple dissolution surfaces within crystal rims. Dacite was still being mixed into the shallow reservoir less than a few months before eruption, supplying the rimless type-1 crystals. Efficient mixing of the two silicic magmas on these timescales is compatible with fluid dynamics principles (Supplementary Discussion). Andesite and basaltic andesite were also injected at a late stage, accounting for small quantities of quenched enclaves discharged during the first eruptive phase[13]. The plagioclase crystals in the rhyodacite have lower Sr isotopic ratios than their host glass[15], so the resident rhyolite may have been more radiogenic than the dacite owing to crustal contamination. The dacite may have been an advance batch of the magmas that have erupted over the last 2,000 yr to form the post-caldera Kameni Islands[13]. This interpretation is based on similarities in An and Sr contents between the cores of type-1 plagioclases and those of plagioclases in the post-caldera lavas[16,17] (Figs 1g and 3c).

Calculations based on chemical mass balance and magma crystallinity show that the dacitic component accounted for at least 15% of the erupted magma (Supplementary Discussion). Assembly of the Minoan reservoir during the 18,000 yr since the previous major eruption of Santorini terminated in a growth spurt involving injection of at least several cubic kilometres of dacitic magma, and an unknown volume of more-mafic magma, in about a century. This implies a transient recharge flux ($>0.05\ \mathrm{km^3\ yr^{-1}}$) much higher than the long-term magma production rate at the volcano[13] ($\sim 0.001\ \mathrm{km^3\ yr^{-1}}$). Rapid and sustained supply of compositionally diverse magmas eventually led to overturn and homogenization of the different magma batches, and eruption followed about a decade later.

Accommodation of such a large recharge volume purely by roof uplift could have caused great inflation of the volcano during the century preceding eruption. A maximum estimate of this is given by the elevation of a rigid, piston-like roof block with the same area as the caldera (several tens of metres of uplift at a mean rate of $\sim 1\ \mathrm{m\ yr^{-1}}$; broader doming of the volcano[18], or consideration of rock and magma compressibilities, would give lower values). Although this is possible, such high uplift values have not been observed, or inferred, before past caldera-forming eruptions such as that of Mt Pinatubo in 1991. However, exhumed granitoid plutons reveal that injection of silicic magma at depths of >3 km is often accommodated by lowering of the intrusion floor due to down-sagging of underlying crystal-rich magmatic mushes and crustal layers[5,19–21]. Extraction of magma from deep storage regions can result in compaction of the crustal column beneath the volcano. Had foundering beneath the Minoan reservoir taken place rapidly enough, precursory uplift might have been greatly reduced. Subsidence rates of several decimetres per year beneath growing magma reservoirs are compatible with theoretical models[5,20].

Our study shows that the reactivation, growth and final assembly of large silicic magma bodies before eruption can take place on decadal to monthly timescales that are very short by comparison with the lengths of the preceding repose periods. It is consistent with evidence for voluminous, late-stage recharge on similar timescales before caldera eruptions elsewhere[11,22–24]. High rates of magma supply sustained over many decades may be necessary to 'prime' such bodies for eruption, by generating overpressures high enough to propagate dykes of viscous magma to the surface and initiate discharge[25,26]. Long-term monitoring of large, dormant caldera systems[27–29], even in remote areas of the world, is essential if late-stage growth spurts of shallow magma reservoirs are to be detected well in advance of caldera-forming eruptions.

Table 1 | Mixing-to-eruption times obtained by diffusion modelling of Mg in Minoan plagioclase

Pumice sample	Eruption phase	Crystal (type)	Time (yr), one-step model	Time (yr), two-step model				
				CIC-dm	CIC-C-R-rm	CIC-R-rm	C-rm	C-R-rm
			900 °C	900 °C	855 °C	855 °C	855 °C	855 °C
S82-30A	1	12 (rimmed 1)	47^{+38}_{-20}	70^{+56}_{-30}	12^{+10}_{-5}	—	—	—
S82-34B	2	A2 (rimmed 1)	$0.8^{+0.6}_{-0.3}$	—	—	—	$0.6^{+0.5}_{-0.3}$	$0.3^{+0.3}_{-0.1}$
R2C	3	B3 (rimmed 1)	60^{+48}_{-26}	60^{+48}_{-26}	—	$<0.9^{+0.8}_{-0.4}$	—	—
S82-11D	4	A6 (rimmed 1)	24^{+20}_{-10}	22^{+17}_{-9}	$0.9^{+0.8}_{-0.4}$	—	—	—
S82-11D	4	A5 (rimless 1)	—	—	—	—	$<0.3^{+0.3}_{-0.1}$	—

The calculations were done at the temperatures shown, which correspond to those of dacitic and rhyodacitic melts. The quoted errors correspond to a temperature uncertainty of +25 °C in the calculated time. CIC, calcic inner core; C, core; R, rim; dm, dacitic melt; rm, rhyodacitic melt. The different crystals are shown in Supplementary Fig. 2.

METHODS SUMMARY

The zoning textures of about 300 crystals from eight pumices (from all four eruptive phases) were studied using a combination of back-scattered electron microscopy and Normarski differential interference contrast microscopy. Major-element compositions of minerals and glasses were analysed by electron microprobe, and trace elements by secondary ion mass spectrometry. The pre-eruptive temperature of the Minoan rhyodacite (853 ± 12 °C) was calculated using analyses of touching magnetite–ilmenite pairs in pumices from all eruptive phases. Trace-element diffusion modelling was carried out in one dimension using a forward modelling approach in which the diffusion equation[12] was solved numerically by a finite-difference scheme, and visual best fits were made between modelled and observed concentration profiles. The An-dependent diffusion coefficient for Mg was taken from ref. 12, which is based on the experimental data of ref. 30, and that for Sr was taken from ref. 31. Initial profiles for Mg were calculated using the Sr–An correlation of Fig. 3c and the Mg–Sr liquid line of descent (Fig. 3b). The boundary conditions were determined by the measured concentrations at the crystal rims or at other major boundary zones. The calculated times are probably overestimates because some of the cores have re-equilibrated significantly and, hence, the effect of diffusion in multiple dimensions could have been significant[7]. However, the main errors associated with the calculations arise from uncertainties in temperature and diffusion coefficients. The modelling was carried out at either 855 or 900 °C, depending on the melt involved (Table 1), but we considered a nominal uncertainty of ±25 °C, which when propagated into the time estimates leads to relative errors of 45–75% (Table 1). Effects of uncertainties in the diffusion parameters for Mg are discussed in Methods.

Full Methods and any associated references are available in the online version of the paper at www.nature.com/nature.

Received 26 May; accepted 4 November 2011.

1. Miller, C. F. & Wark, D. A. Supervolcanoes and their explosive supereruptions. *Elements* **4,** 11–15 (2008).
2. Newhall, C. G. & Dzurizin, D. *Historical Unrest at Large Calderas of the World* Vols 1 and 2 (Bull. US Geol. Surv. 1855, USGS, 1988).
3. Gottsmann, J. & Marti, J. (eds) *Caldera Volcanism: Analysis, Modelling and Response* (Dev. Volcanol. 10, Elsevier, 2008).
4. Sigurdsson, H. & Carey, S. and 12 others. Marine investigations of Greece's Santorini volcanic field. *Trans. Am. Geophys. Union* **87,** 337–342 (2006).
5. Bachmann, O. & Bergantz, G. W. On the origin of crystal-poor rhyolites: extracted from batholithic crystal mushes. *J. Petrol.* **45,** 1565–1582 (2004).
6. Burgisser, A. & Bergantz, G. W. A rapid mechanism to remobilize and homogenize highly crystalline magma bodies. *Nature* **471,** 212–215 (2011).
7. Costa, F., Dohmen, R. & Chakraborty, S. Timescales of magmatic processes from modeling the zoning patterns of crystals. *Rev. Mineral. Geochem.* **69,** 545–594 (2008).
8. Bindeman, I. N., Davis, A. M. & Drake, M. J. Ion microprobe study of plagioclase-basalt partition experiments at natural concentration levels of trace elements. *Geochim. Cosmochim. Acta* **62,** 1175–1193 (1998).
9. Blundy, J. & Wood, B. Crystal-chemical control on the partitioning of Sr and Ba between plagioclase feldspar, silicate melts, and hydrothermal solutions. *Geochim. Cosmochim. Acta* **55,** 193–209 (1991).
10. Zellmer, G. F., Blake, S., Vance, D., Hawkesworth, C. & Turner, S. Plagioclase residence times at two island arc volcanoes (Kameni Islands, Santorini, and Soufriere, St Vincent) determined by Sr diffusion systematics. *Contrib. Mineral. Petrol.* **136,** 345–357 (1999).
11. Morgan, D. J. *et al.* Magma chamber recharge at Vesuvius in the century prior to the eruption of A.D. 79. *Geology* **34,** 845–848 (2006).
12. Costa, F., Chakraborty, S. & Dohmen, R. Diffusion coupling between trace and major elements and a model for calculation of magma residence time using plagioclase. *Geochim. Cosmochim. Acta* **67,** 2189–2200 (2003).
13. Druitt, T. H. *et al. Santorini Volcano* (J. Geol. Soc. Lond. Mem. 19, Geological Society, 1999).
14. Cottrell, E., Gardner, J. E. & Rutherford, M. J. Petrologic and experimental evidence for the movement and heating of the pre-eruptive Minoan rhyodacite (Santorini, Greece). *Contrib. Mineral. Petrol.* **135,** 315–331 (1999).
15. Martin, V., Davidson, J., Morgan, D. & Jerram, D. Using the Sr isotope compositions of feldspars and glass to distinguish magma system components and dynamics. *Geology* **38,** 539–542 (2010).
16. Francalanci, L. *et al.* in *The European Laboratory Volcanoes* 175–186 (Official Publ. Eur. Comm., 1998).
17. Huijsmans, J. *Calc-Alkaline Lavas from the Volcanic Complex of Santorini, Aegean Sea, Greece* (Geologica Ultraiectina 41, Inst. Aardwetenschappen Rijksuniversiteit Utrecht, 1985).
18. Aizawa, K., Acocella, V. & Yoshida, T. How the development of magma chambers affects collapse calderas: insights from an overview. *Spec. Publ. Geol. Soc. (Lond.)* **269,** 65–81 (2006).
19. Wiebe, R. A. & Collins, W. J. Depositional features and stratigraphic sections in granitic plutons: implications for the emplacement and crystallization of granitic magma. *J. Struct. Geol.* **20,** 1273–1289 (1998).
20. Cruden, A. R. On the emplacement of tabular granites. *J. Geol. Soc. Lond.* **155,** 853–862 (1998).
21. Grocott, J. Arévalo, C. Welkner, D. & Cruden, A. Fault-assisted vertical pluton growth: Coastal Cordillera, north Chilean Andes. *J. Geol. Soc. Lond.* **166,** 295–301 (2009).
22. Wark, D. A., Hildreth, W., Spear, F. S., Cherniak, D. J. & Watson, E. B. Pre-eruption recharge of the Bishop magma system. *Geology* **35,** 235–238 (2007).
23. Saunders, K. E., Morgan, D. J., Baker, J. A. & Wysoczanski, R. J. The magmatic evolution of the Whakamaru supereruption, New Zealand, constrained by a microanalytical study of plagioclase and quartz. *J. Petrol.* **51,** 2465–2488 (2010).
24. de Silva, S., Salas, G. & Schubring, S. Triggering explosive eruptions: the case for silicic magma recharge at Huaynaputina, southern Peru. *Geology* **36,** 387–390 (2008).
25. McLeod, P. & Tait, S. R. The growth of dykes from magma chambers. *J. Volcanol. Geotherm. Res.* **92,** 231–245 (1999).
26. Jellinek, A. M. & DePaulo, D. J. A model for the origin of large silicic magma chambers: precursors of caldera-forming eruptions. *Bull. Volcanol.* **65,** 363–381 (2003).
27. Gottsmann, J. & Battaglia, M. Deciphering causes of unrest at explosive collapse calderas: Recent advances and future challenges of joint time-lapse gravimetric and ground deformation studies. *Dev. Volcanol.* **10,** 417–446 (2008).
28. Hill, D. P. Unrest in Long Valley caldera, California, 1978–2004. *Spec. Publ. Geol. Soc. (Lond.)* **269,** 1–24 (2006).
29. Dzurisin, D., Yamashita, K. M. & Kleinman, J. W. Mechanisms of crustal uplift and subsidence at the Yellowstone caldera, Wyoming. *Bull. Volcanol.* **56,** 261–270 (1994).
30. LaTourrette, T. & Wasserbourg, G. J. Mg diffusion in anorthite: implications for the formation of early solar system planetismals. *Earth Planet. Sci. Lett.* **158,** 91–108 (1998).
31. Giletti, B. J. & Casserly, J. E. D. Strontium diffusion kinetics in plagioclase feldspars. *Geochim. Cosmochim. Acta* **58,** 3785–3793 (1994).
32. Santo, A. P. Magmatic evolution processes as recorded in plagioclase phenocrysts of Nea Kameni rocks (Santorini Volcano, Greece). *Dev. Volcanol.* **7,** 139–160 (2005).

Supplementary Information is linked to the online version of the paper at www.nature.com/nature.

Acknowledgements This study was funded partly by the French Agence National de Recherche (ANR STOMIXAN, contract no. ANR-08CEA080, to B.S.). We are grateful to R. Armstrong, P. Crançon and R. Girardin for their contributions during the early stages of this study, and to J. Blundy and M. Reid for reviews. This is Laboratory of Excellence ClerVolc contribution no. 1.

Author Contributions T.H.D. defined the project strategy, analysed the data and wrote the first draft of the manuscript, which was then revised by all the authors. E.D., M.D. and T.H.D. made the trace-element analyses, F.C. did the diffusion modelling and B.S. performed the fluid dynamic calculations.

Author Information Reprints and permissions information is available at www.nature.com/reprints. The authors declare no competing financial interests. Readers are welcome to comment on the online version of this article at www.nature.com/nature. Correspondence and requests for materials should be addressed to T.H.D. (t.druitt@opgc.univ-bpclermont.fr).

METHODS

Sample preparation and analysis. Plagioclase crystals (250–400-μm and 400–700-μm size fractions) from eight pumices from all four eruptive phases[13] were mounted in epoxy resin, mostly on (010), then polished. The zoning textures of about 300 crystals were studied using a combination of back-scattered electron microscopy and Normarski differential interference contrast microscopy. Sectioning through the centres of the crystals was ensured by visual observation using a binocular microscope and by rejection of zoning images that were evidently oblique cuts. Major-element compositions of plagioclase were analysed using a Cameca SX100 electron microprobe at an accelerating voltage of 15–20 kV and beam current of 8–15 nA. The pre-eruptive temperature of the Minoan rhyodacite (853 ± 12 °C) was calculated using analyses of touching magnetite–ilmenite pairs in pumices from all eruptive phases, the recalculation procedure of ref. 33, and the thermometer of ref. 34.

Abundances of a number of isotopes as far up the periodic table as ^{140}Ce, including ^{24}Mg, ^{47}Ti and ^{88}Sr, were analysed using two ion probes: a Cameca IMS 4f instrument at the University of Edinburgh (4.5–5-nA primary O^- beam) and a Cameca IMS 1280 instrument at the CRPG, Nancy (14–20-nA primary O^- beam), using beam diameters of 10–15 μm and calibrated against glass standards NBS 6104 and ML3B-G. Secondary ions were energy-filtered using band passes of 100 and 35 V, offsets of 100 and 60 V, and mass resolutions of 300 and 5,000 on the IMS 4f and the IMS 1280, respectively, following a short pre-sputtering period. Only high-energy ions were measured, to reduce the matrix effect on relative ion yields[35]. The calibration line for Sr, including glass standards StHs, KL2G, TIG BHVO and BCR2G, and CRPG reference albite and plagioclase, shows no matrix effect for a large range of glass and mineral compositions. Isotope concentrations were expressed as ratios relative to ^{30}Si, and were then corrected using electron microprobe analyses of Si contents adjacent to the ion probe pits. The relative ionization yields were determined on glass standards. Internal precisions (mean relative deviation) on the ion/^{30}Si ratios for each spot analysis were typically better than 5% for Mg, 5% for Sr and 10% for Ti. Values for all elements on the IMS 4f were systematically slightly lower than those on the IMS 1280, and were raised using a small multiplication factor.

Selected profiles were also analysed for Mg using a Cameca SX100 electron microprobe (accelerating voltage, 15 kV; beam current, 40 nA; total counting time per spot, 50 s), and using a LA-ICP-MS system consisting of a 193-nm excimer (ArF) laser-ablation system (M50, Resonetics) coupled to an Agilent 7500CS ICP-MS (10-μm beam size; 6-mJ beam energy; 1-Hz repetition rate). Results from the three techniques agreed to within 25%.

Crystal–melt trace-element partitioning. We used the An-dependent partition functions in ref. 8 for Mg, Sr and Ti. The Sr partition function in ref. 9 gives results within a few per cent of that in ref. 8. The partition functions for Mg, Sr and Ti in ref. 8 seem to work well for Santorini compositions. There is good agreement between the contents of Sr and Ti in the crystal rims and the plagioclase compositions calculated to be in equilibrium with the interstitial glasses (Fig. 2). Agreement for Mg is not as good, although the disparity is small in comparison with the overall range of this element in Santorini plagioclases and melts (Figs 2 and 3b). Strontium and Ti contents of the calcic inner cores of Minoan plagioclase crystals agree with those predicted in ref. 8 to be in equilibrium with Santorini basaltic and basaltic andesite melts (Fig. 3a). Magnesium contents of calcic plagioclase occurring in Santorini basalts and basaltic andesites[36–38] agree with the Mg contents of those rocks (Fig. 3b) using the Mg partition coefficient in ref. 8.

Diffusion modelling. Diffusion modelling was carried out using the method of ref. 12 with distance increments of 3.5–5.3 μm. We used the Mg diffusion coefficient in plagioclase in ref. 12, which is based on the experimental data in ref. 30:

$$D_{Mg} = \left[2.92 \times 10^{-4.1X_{An}-3.1} \exp\left(\frac{-266{,}000}{RT}\right)\right] \quad (1)$$

The diffusion coefficient for Sr was taken from ref. 31:

$$D_{Sr} = \left[2.92 \times 10^{-4.1X_{An}-4.08} \exp\left(\frac{-276{,}000}{RT}\right)\right] \quad (2)$$

In these expressions, D is the element diffusion coefficient in $m^2 s^{-1}$, X_{An} is the mole fraction of anorthite, T is the temperature in kelvin and R is the ideal gas constant. According to equations (1) and (2), $D_{Mg} > D_{Sr}$ at all temperatures in plagioclase of a given An content. We used the equation for trace-element diffusion in plagioclase derived in ref. 12, which takes into account the effect of An content on equilibrium profile shapes and diffusion coefficients:

$$\frac{\partial C_i}{\partial t} = \left(D_i \frac{\partial^2 C_i}{\partial x^2} + \frac{\partial C_i}{\partial x}\frac{\partial D_i}{\partial x}\right) - \frac{A}{RT}\left(D_i \frac{\partial C_i}{\partial x}\frac{\partial X_{An}}{\partial x} + C_i \frac{\partial D_i}{\partial x}\frac{\partial X_{An}}{\partial x} + D_i C_i \frac{\partial^2 X_{An}}{\partial x^2}\right)$$

Here A is a thermodynamic factor that relates the dependence of the partition coefficient on the An content[8], x is distance, C is concentration and t is time.

We used two temperatures in the modelling: 900 °C for models in which the host melt was dacitic and 855 °C for those in which it was rhyodacitic (Table 1). These temperatures are constrained by the temperature (855 °C) of the magma on eruption (from touching pairs of Fe-Ti oxides), and are consistent with the formula used for plagioclase–melt element partitioning (Fig. 3).

The equilibrium distributions of Mg, Sr and Ti within the plagioclase crystals were obtained as follows. We first calculated the plagioclase–melt partition coefficients using the measured An contents and the equations in ref. 8. Using the partition coefficients, and the measured trace-element concentrations at the crystal rims, we then calculated a melt composition in equilibrium with the rim. Finally, the composition of the entire plagioclase crystal in equilibrium with the calculated melt (and crystal rim) was calculated using the partition coefficient for each portion of the crystal.

The initial Mg profile was estimated using the Sr–An correlation of Fig. 3c and the Mg–Sr liquid line of descent (Fig. 3b). The relationship between the initial Mg and An contents used in the modelling is $[Mg] = 48.2\exp(2.9X_{An})$, where the concentration of Mg (left-hand side) is measured in p.p.m. This approach is justified because the times involved in the processes are short enough not to have affected Sr concentrations in any significant manner. The uncertainty in the initial Mg content shown in Fig. 2 was estimated by error propagation. For the boundary conditions, we used measured concentrations at the rims of the crystals or at the appropriate boundary between two crystal zones in the multiple-step models.

In the modelling, we explored two endmember possibilities. The first is to model the entire crystal, including the rim, core and calcic inner core, all at once (one-step model) at 900 °C. This is equivalent to assuming that diffusion started only after the crystal was fully grown, and is the approach of all previously published models using plagioclase. This should not be a bad approximation if the diffusion time is relatively long and if growth rates are relatively high. The second possibility is to model the crystal piece by piece; for example, first model equilibration of the calcic inner core with dacitic melt at 900 °C, then add the core, rim and rhyodacitic melt at 855 °C, and continue diffusing (two-step model). This is a first-order approximation for modelling simultaneous crystal growth and diffusion. We tried both approaches, and in most cases there were no significant differences in total times, but the fits to the data were better when we used the two-step approach. This also gave us additional information about the timescales of different processes recorded in different parts of the crystals. To our knowledge this is the first time that plagioclase zoning has been used to provide chronologies of multiple events from single crystals. We note that to model some crystals successfully, we needed to use a condition where Mg in the crystal was already equilibrating with the host melt before any subsequent overgrowth by a new composition.

We illustrate the two approaches using crystal S82-30A 12 (Supplementary Fig. 5). We were not able to obtain a good fit to the measured Mg profiles using a one-step model, which gave an approximate time of 47 yr. We therefore modelled the diffusion using the two-step approach. We first did an equilibration of the calcic inner core with dacitic melt at 900 °C, and obtained a time of 70 yr (step 1 of Supplementary Fig. 4b). We then added the core and rim over the calcic inner core and continued to diffuse in rhyodacitic melt at 855 °C, and obtained a further time of 12 yr (step 2 of Supplementary Fig. 5b). The total time recorded by the crystal is therefore 82 yr, with a fit that is clearly better than in a one-step approach. We also tried more detailed models involving, for example, three steps (inner core/melt, inner core/core/melt and inner core/core/rim/melt), but the results were virtually identical to those of the two-step model.

In the case of the rimless type-1 crystal (S82-11D A5), the composition of which is out of equilibrium with the host rhyodacitic melt, we modelled the time necessary for Mg and Sr in the outer 25 μm of the crystal to be significantly modified by diffusive re-equilibration. The times at 855 °C were 0.3 yr for Mg (Table 1) and 12 yr for Sr. The crystal therefore cannot have resided in the melt for longer than 0.3 yr.

The times obtained from Mg diffusion calculations are subject to various types of uncertainty[7]. First, the temperatures obtained from geothermometers have errors of about ±25 °C, which when propagated into the time estimates lead to the relative uncertainties given in Table 1. Second, the diffusion calculations were carried out in one dimension, which has been shown to overestimate actual (three-dimensional) diffusion time[7] when the extent of diffusion is as significant as that shown by some of the inner cores of our crystals. Third, uncertainty arises from experimentally determined diffusion coefficients. Magnesium diffusion in

plagioclase was measured in An_{95} and at 1,200–1,400 °C (ref. 30), and the measurements are precise to within a factor of two. Following ref. 12, equation (1) assumes that the activation energy and pre-exponential factor determined for D_{Mg} at higher temperatures applies at 900 °C. Down-temperature extrapolation of diffusion data is common practice and a necessity in almost all studies that use experimentally determined diffusion coefficients to model natural processes[39,40]. This is because the experimental times required to produce significant profiles to determine diffusion coefficients are impracticably long (but see ref. 41). The extrapolation is not a significant problem if there is no change of the diffusion mechanism (which would imply a change in the activation energy) at lower temperatures. There have been many determinations of other cation diffusivities[42] (for example those of Sr, Li and Ca) in plagioclase feldspars over wide ranges of temperature (including 900 °C), and these do not show kinks in activation energy.

There is also uncertainty in the An dependence in equation (1), which assumes that the An dependence of Mg diffusion is the same as that of Sr (ref. 12). This assumption was used in ref. 12 because only certain dependencies are possible if good fits to the natural data are to be obtained. In addition to this observation, we have here estimated an uncertainty due to the An dependence term in equation (1) by combining natural data and the well-calibrated Sr diffusivities. The data in Table 1 and Fig. 2, as well as those published elsewhere[7,43,44], show that the degree of equilibration of Mg is always higher than that of Sr, irrespective of An content. This means that $D_{Mg} > D_{Sr}$ not only for An_{95} (ref. 30) but for all An contents. Thus, the dependence of D_{Mg} on An cannot be too low because otherwise $D_{Sr} > D_{Mg}$ at low An content. Using this constraint, and equation (2) for D_{Sr}, the minimum possible dependence on An (that is, the first exponent) in equation (1) has the form $-2.6X_{An} - 4.53$, which in a plot of D_{Mg} versus %An (Supplementary Fig. 6) gives a much lower slope than that given by equation (1). The effect that this has on the times ranges from an increase by a factor of two in the one-step fit for crystal R2C B3 (130 yr) to an increase by a factor of three for crystal 34BA2 (2.3 yr). We conclude that the uncertainty in this parameter does not increase the times in Table 1 by more than about a factor of three.

We also carried out diffusion modelling of Sr (for which the diffusion parameters are very well constrained[31]; Fig. 2), to gain first-order independent constrains on the timescales inferred from Mg. For this, we assumed that the observed profiles were near primary and carried out one-step diffusion models at 900 °C to see what times were required for significant perturbation of those profiles. The results (Fig. 2) show that crystal residence times longer than a couple of hundred years would significantly blur the tight relationship between plagioclase Sr and An content (Fig. 3c), and are therefore excluded.

Finally, there is also an uncertainty in the determination of the best fits of the model and measured concentrations, which include the analytical errors. The fits were done visually because, given the complexity of the natural profiles, it does not make sense to implement least-squares routines. The uncertainty from this varies from crystal to crystal and ranges from less than 10% for crystals that have been largely equilibrated (for example by step one of most crystals) to up to 40% for step two, where concentrations vary by a small amount and may be close to the initial values (for example in crystal S82-34B A2).

33. Stormer, J. C. Jr. The effects of recalculation on estimates of temperature and oxygen fugacity from analyses of multicomponent iron-titanium oxides. *Am. Mineral.* **68,** 586–594 (1983).
34. Andersen, D. J. & Lindsley, D. H. New (and final!) models for the Ti-magnetite/ilmenite geothermometer and oxygen barometer. *Trans. Am. Geophys. Union* **66,** 416 (1985).
35. Hinton, R. W. Ion microprobe trace-element analysis of silicates: measurement of multi-element glasses. *Chem. Geol.* **83,** 11–25 (1990).
36. Vaggelli, G., Pellegrini, M., Vougioukalakis, G., Innocenti, S. & Francalanci, L. Highly Sr radiogenic tholeiitic magmas in the latest inter-Plinian activity of Santorini volcano, Greece. *J. Geophys. Res.* **114,** B06201 (2009).
37. Conticelli, S., Francalanci, L., Santo, A. P. & Petrone, C. in *The European Laboratory Volcanoes* 157–174 (Official Publ. Eur. Comm., 1998).
38. Gertisser, R., Preece, K. & Keller, J. The Plinian lower pumice 2 eruption, Santorini, Greece: magma evolution and volatile behaviour. *J. Volcanol. Geotherm. Res.* **186,** 387–406 (2009).
39. Lasaga, A. C. *Kinetic Theory in the Earth Sciences* (Princeton Univ. Press, 1998).
40. Zhang, Y. Diffusion in minerals and melts: theoretical background. *Rev. Mineral. Geochem.* **72,** 5–59 (2010).
41. Dohmen, R., Becker, H.-W., Meißner, E., Etzel, T. & Chakraborty, S. Production of silicate thin films using pulsed laser deposition (PLD) and applications to studies in mineral kinetics. *Eur. J. Mineral.* **14,** 1155–1168 (2002).
42. Cherniak, D. Cation diffusion in feldspars. *Rev. Mineral. Geochem.* **72,** 691–733 (2010).
43. Costa, F., Coogan, L. & Chakraborty, S. The time scales of magma mixing and mingling involving primitive melts and melt–mush interaction at mid-ocean ridges. *Contrib. Mineral. Petrol.* **159,** 371–387 (2010).
44. Costa, F. & Morgan, D. in *Timescales of Magmatic Processes: from Core to Atmosphere* (eds Dosseto, A., Turner, S. P. & Van Orman, J. A) 125–159 (Wiley-Blackwell, 2010).